

Defects passivation and crystal growth promotion by solution-processed K doping strategy toward 16.02% efficiency Cu(In,Ga)(S,Se)2 solar cells

Y.-H. Zhao, Q.-Q. Gao, S.-J. Yuan, Q.-Q. Chang, T. Liang, Z.-H. Su, H.-L. Ma, S. Chen, G.-X. Liang, P. Fan, et al.

▶ **To cite this version:**

Y.-H. Zhao, Q.-Q. Gao, S.-J. Yuan, Q.-Q. Chang, T. Liang, et al.. Defects passivation and crystal growth promotion by solution-processed K doping strategy toward 16.02% efficiency Cu(In,Ga)(S,Se)2 solar cells. Chemical Engineering Journal, 2022, 436, pp.135008. 10.1016/j.cej.2022.135008 . hal-03596450

HAL Id: hal-03596450
https://hal.science/hal-03596450

Submitted on 1 Apr 2022

HAL is a multi-disciplinary open access archive for the deposit and dissemination of scientific research documents, whether they are published or not. The documents may come from teaching and research institutions in France or abroad, or from public or private research centers.

L'archive ouverte pluridisciplinaire **HAL**, est destinée au dépôt et à la diffusion de documents scientifiques de niveau recherche, publiés ou non, émanant des établissements d'enseignement et de recherche français ou étrangers, des laboratoires publics ou privés.



Distributed under a Creative Commons Attribution - NonCommercial 4.0 International License

Defects Passivation and Crystal Growth Promotion by Solution-Processed K Doping Strategy toward 16.02% Efficiency Cu(In,Ga)(S,Se)$_2$ Solar Cells

Yun-Hai Zhao[a, b, c, 1], Qian-Qian Gao[a, 1], Sheng-Jie Yuan[a, *], Qian-Qian Chang[a], Ting Liang[a], Zheng-Hua Su[b], Hong-Li Ma[c], Shuo Chen[b], Guang-Xing Liang[b], Ping Fan[b], Xiang-Hua Zhang[c], and Si-Xin Wu[a, *]

[a]Key Laboratory for Special Functional Materials of MOE, National & Local Joint Engineering Research Centre for High-efficiency Display and Lighting Technology, School of Materials, Henan University, Kaifeng, 475004, P. R. China

[b]Shenzhen Key Laboratory of Advanced Thin Films and Applications, Key Laboratory of Optoelectronic Devices and Systems, College of Physics and Optoelectronic Engineering, Shenzhen University, Shenzhen, 518060, P. R. China

[c]Univ Rennes, CNRS, ISCR (Institut des Sciences Chimiques de Rennes) UMR 6226, Rennes, F-35000, France

*Corresponding author

E-mail address: yuanshengjie@vip.henu.edu.cn (S.-J. Yuan); wusixin@henu.edu.cn (S.-X. Wu)

Yun-Hai Zhao and Qian-Qian Gao contributed equally to this work.

Abstract

Unsatisfactory crystal quality and deep-level defects are detrimental for Cu(In,Ga)(S,Se)$_2$ (CIGSSe) solar cells. In this work, an in-suit K doping strategy is implemented by introducing KF into the CIGSSe precursor solution to promote crystallization and passivate the deep defects. The effects of K on the

Journal Pre-proofs

solution-processed CIGSSe devices are systematic investigated. It has been discovered that K incorporation results in better crystallization, modified CIGSSe surface and fewer detrimental defects. Benefit from the reduction of the band-tailing effects, suppressed defects density and passivated interface recombination, the solution-processed CIGSSe solar cell achieve systematic improvement in open-circuit voltage and fill factor, enabling a champion efficiency of 16.02%, which is the highest value for alkali metal doped CIGSSe solar cells fabricated by solution-processed method. The effective in-suit K doping tactic opens an avenue for developing highly efficient solution-processed CIGSSe solar cells.

Keywords: $Cu(In,Ga)(S,Se)_2$, potassium doping, solar cells, solution processing, defects passivation.

1. Introduction

The demand for high-efficiency and low cost solar cells is always the driving force for thin film photovoltaics. Sustained research on new absorbers such as $CuFeSe_2$,[1] Sb_2Se_3,[2] GeSe [3] and $CsPbBr_3$ [4] et.al have achieved great progress in devices performances. Among them, the chalcopyrite $Cu(In,Ga)(S,Se)_2$ (CIGSSe) has been considered as the most promising absorber material for thin-film solar cells because of its high efficiency, low cost, and long-term durability.[5-7] World record efficiency of 23.35% is obtained by Solar Frontier, which is comparable to the leading silicon solar cells in the photovoltaic market.[8] However, there remained challenges which inhibited the commercialization process of CIGSSe. High efficiencies CIGSSe solar cells are commonly prepared through vacuum deposition process such as sputtering

Journal Pre-proofs

and co-evaporation.[8-10] These processes need complex vacuum technologies and facilities, which increase manufacturing cost. Therefore, it is highly desirable to develop low-cost and simple CIGSSe thin film deposition methods to reduce the production cost.

Solution processing methods have been emerged as attractive alternatives to vacuum based methods because it exhibits inherent high material utilization, low cost, and high throughput fabrication.[11-13] In recent years, a variety of solution processed CIGSSe solar cells based on different solvent systems such as hydrazine, amine-thiol, DMF, DMSO and methanol have obtained power conversion efficiencies up to 15%.[5, 6, 11, 14-16] These efficiencies have reached the threshold for commercial applications, demonstrating its high potential. Nevertheless, since the CIGSSe device efficiency reached 17.3% in 2016, the efficiency gap between vacuum-processed device and solution-processed device is widening.[11] The inferior efficiencies of solution-processed CIGSSe devices are often attributed the impurities, poor crystal quality, band tailing and deep-level defects.[5, 17-20] For vacuum based CIGSSe devices, the introduction of alkali metal post-deposition treatments (PDT) had played a crucial role in the history of efficiency improvement of CIGSSe solar cells.[13, 21-23] The light alkali metal (Na) doping of CIGSSe absorber can passivate grain boundaries, increase the carrier concentration, reduce point defects and promote the crystal growth of the absorber.[20] Otherwise, heavier alkali metal (K, Rb, Cs) doping can widen the CIGSSe surface bandgap and enhances charge selectivity.[9, 24, 25] Despite alkali metal doping has so many advantages, limited attempts have been

carried out in solution-processed CIGSSe solar cells. Ulicná et al. thermal evaporated a thin layer of NaCl on the top of CIGSSe precursor films to fabricate CIGSSe device with PCE of 10.3%.[26] This result shows that Na-doped CIGSe absorber has larger grains. Rehan et al. also observed enlarged CIS grain size with Na doping.[20] They found that Na doping could increase the J_{SC} of the solution-processed devices, whereas Na has little effect on the J_{SC} of the vacuum-processed devices. Alruqobah et al. evaporated NaF and KF onto the as-coated sulfide CIGSSe nanoparticle films to obtain CIGSSe devices with 12.0% PCE, and revealed that K-CIGSSe films have larger grains and high-bandgap K-In-Se surface phase.[27] Min group intentionally introduced a K layer within the multi-layered Cu-In-Ga oxide precursor film through solution processing to boost Se penetration during chalcogenization, thus achieving CIGSSe solar cell with the efficiency of 15.0%.[28] Lu et al. found that the incorporation of potassium ions into CIGSSe films can diminish the formation of detrimental $Cu_{2-x}Se$ phase, which improved the device efficiency from 4.70% to 11.02%.[29] Although these experimental studies have demonstrated the positive role of alkali metal in solution-processed CIGSSe solar cells, the essence of the interaction between alkali metal and efficiency enhancement still needs to be further studied and the underlying mechanism has not been entirely clear. In addition, during the solution-based film growth process, there are many uncertain factors surrounding the interaction of alkali elements with the main elements and/or various point defects in the absorber film. Hence, the alkali metal treatment effects on the solution-processed CIGSSe absorber need be re-investigated to provide guidance to suppress carrier

recombination in solution-processed CIGSSe absorber and improve CIGSSe device performance.

Because of the medium size of K atom, K doping is supposed to have both the advantages of light alkali metals and heavy alkali metals, that is, simultaneously modifying both the CIGSSe bulk properties and CIGSSe surface properties.[24, 28] In this work, in-suit K doping strategy was utilized by simply dissolving KF into the CIGSSe precursor solution. Through this strategy, the content of K can be easily adjusted. We systematically explored the effects of K ions in the microstructure, electrical and defects properties of CIGSSe films. We found that the incorporation of K leads to improved crystallization, reduced defect density, and improved interface carrier transportation. We claimed that our process offers a simple and cost-effective method for fabricating highly efficient CIGSSe devices. Meanwhile it also helps us to further understand the deep reason behind the efficiency promotion of CIGSSe devices.

2. Experimental Section

2.1. Precursor film deposition and selenization

The precursor solution was prepared according to our previous reports. In brief, 0.1273 g Cu powder, 0.1622 g In powder, 0.0530 g Ga powder, and 0.3400 g Se powder were dissolved in the mixture of ethylenediamine (7.20 mL) and 1,2-ethanedithiol (0.72 mL), and then stirred at 70 ^{o}C for 24 h to get a homogeneous brown solution. In our previous work, the as-prepared CIGSSe absorber included a little amount sulfur element, which was resulted from the 1,2-ethanedithiol solvent

Journal Pre-proofs

(Molecular formula: $C_2H_6S_2$) solvent.[30] The as-prepared absorber was labeled as $Cu(In,Ga)(S,Se)_2$ (CIGSSe). To study the effect of K in CIGSSe film, K was added directly into the CIGSSe precursor solution using KF as potassium source (Fig. S1). The molar ratios of K to Cu element were 1, 5 and 10 mol‰, respectively. The precursor solution was spin-coated on Mo substrate 3000 rpm for 30 s, following a sintering process on a 350 ^oC hot plate for 2 min. The same process was repeated ten times to obtain desired film thickness. Then the as-prepared CIGSSe precursor films with and without KF were putted into graphite box and selenized in rapid thermal processing (RTP) furnace with nitrogen flowing. Selenium particles (80 mg) were utilized as Se source. The selenization process was shown in Figure S2. Firstly, the heating temperature was raised from room temperature to 550 °C within 60 s and maintained at 550 °C for 900 s. After that, the RTP furnace was naturally cooled to room temperature.

2.2. Device fabrication

60 nm CdS buffer layer was deposited on the as-prepared CIGSSe absorber through chemical bath deposition (CBD) method. Then, i-ZnO (50 nm) and ITO (150 nm) were subsequently deposited by sputtering process. 70-nm thick Ag electrode was successively deposited on the top of the device using thermal evaporation. Finally, the CIGSSe devices were covered with MgF_2 (100 nm) anti-reflection coating by thermally evaporation. The active area of each CIGSSe solar cell was 0.21 cm^2.

2.3. Characterization

The crystalline phases of the obtained films were examined using X-ray

Journal Pre-proofs

diffractometer (XRD, Bruker D8 Advance) at 40 kV and 40 mA. The scanning electron microscopy (SEM) images were recorded using a field emission SEM (Nova Nano SEM 450, FEI, USA). XPS studies were performed using a ESCALAB 250 XPS system (Thermo Fisher Scientific) with a monochromatized Al anode X-ray source. Elemental depth compositional profiles of the devices were determined by The TOF SIMS 5 secondary-ion mass spectrometry (SIMS) workstation (IONTOF GmbH). The J-V characteristics were acquired under a simulated standard test condition of illumination intensity (Zolix SS150) under a simulated air mass of 1.5 global by using a source measurement unit (Keithley 2400) with four-terminal sensing. The EQE values were obtained using a Zolix SCS100 QE system. Capacitance-voltage (C-V) and DLCP were measured by a Keithley 4200A-SCS system with JANIS cryogenic platform. Deep level transient spectra (DLTS) were obtained by an FT-1030 HERA DLTS system configured with a JANIS VPF-800 cryostat controller. J-V-T curve was measured using HERA-DLTS system (Phys Tech) configured with a JANIS VPF-800 cryostat controller under dark condition. J-V-T characteristics were recorded in steps of 10 K after temperature stabilization while cooling down from 350-90 K set temperature. The transient surface photovoltage measurements were carried out with a Nd:YAG pulsed laser (355 nm and 4 ns, Quantel Brilliant Eazy, BRILEZ/IR-10) and a digital oscilloscope (500MHz, TDS 3054C, Tektronix). Solar cells were placed into a SEM vacuum chamber to implement EBIC measurements (Gatan, Inc.). The electron-beam voltage was 20 kV.

3. Results and Discussions

Journal Pre-proofs

Fig. 1 showed the schematic diagram for the preparation process of K doped CIGSSe thin films. The optimum K content for solution-processed CIGSSe absorber can be easily optimized by adjusting the amount of added K source in CIGSSe precursor solution. For clarity, CIGSSe absorbers prepared through KF solutions with 0, 1, 5 and 10 mol‰ concentration were defined as K0, K1, K5 and K10, respectively.

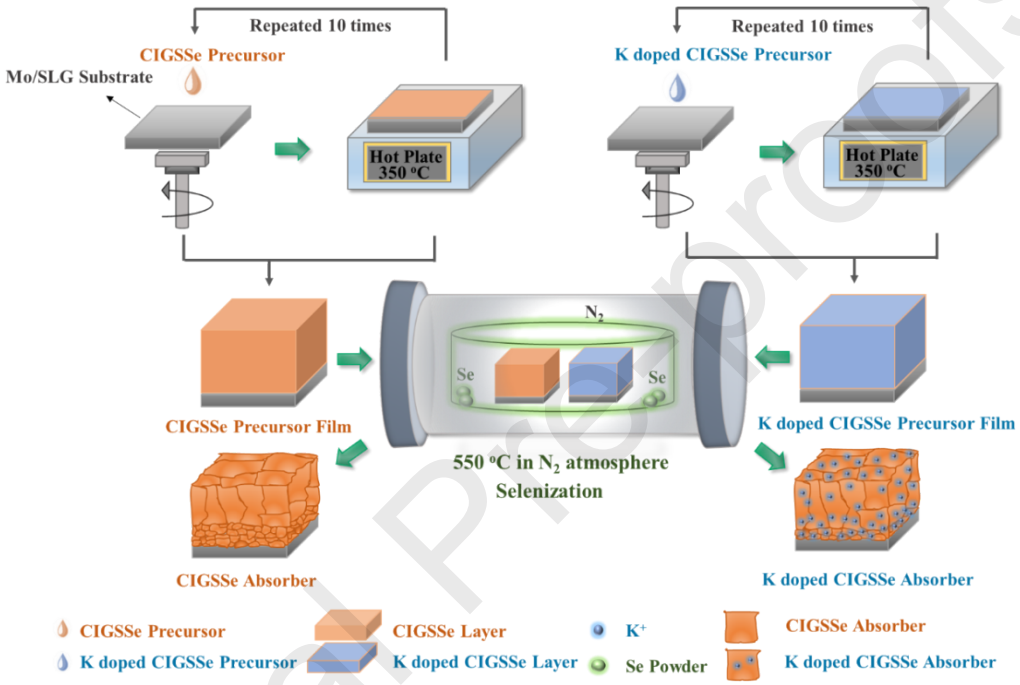


Fig. 1 Schematic diagram of the preparation process of CIGSSe absorber and K doped CIGSSe absorber.

The influence of K introduction on crystal structure of the CIGSSe films was first investigated. As shown in Fig. 2, the diffraction peaks located at 40.4° and 31.8° can be assigned to the characteristic of Mo and $MoSe_2$, indicating the Mo layer was partly selenized.[31] The other diffraction peaks can be ascribed to the polycrystalline chalcopyrite CIGSSe structure.[6, 19] In magnified XRD patterns (Fig. 2b), the main peak positions with (112) plane of all samples were nearly unchanged. The introduced K in CIGSSe films might well tend to locally accumulated at the grain boundaries, while a small amount K was distributed within the CIGSSe grains.[32, 33] The host

crystal structure of the CIGSSe films was little affected by the K incorporation and thus the XRD peak position was not shifted. The (112) peak intensity of K-doped CIGSSe was higher and the full width at half maximum (FWHM) of (112) peak was smaller than K-free CIGSSe film. The stronger XRD intensities and smaller FWHM were indicative of improved crystalline quality and larger grain size.[34]

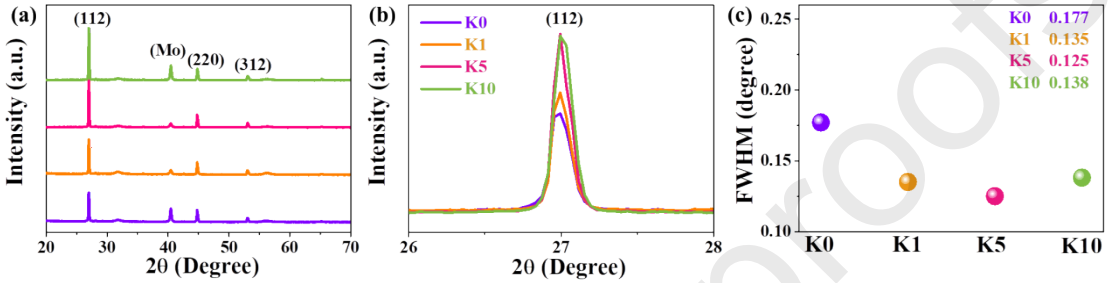


Fig. 2 (a) XRD patterns of sample K0-K10; (b) enlarged image of the (112) crystal plane; (c) The FWHD of the (112) crystal plane.

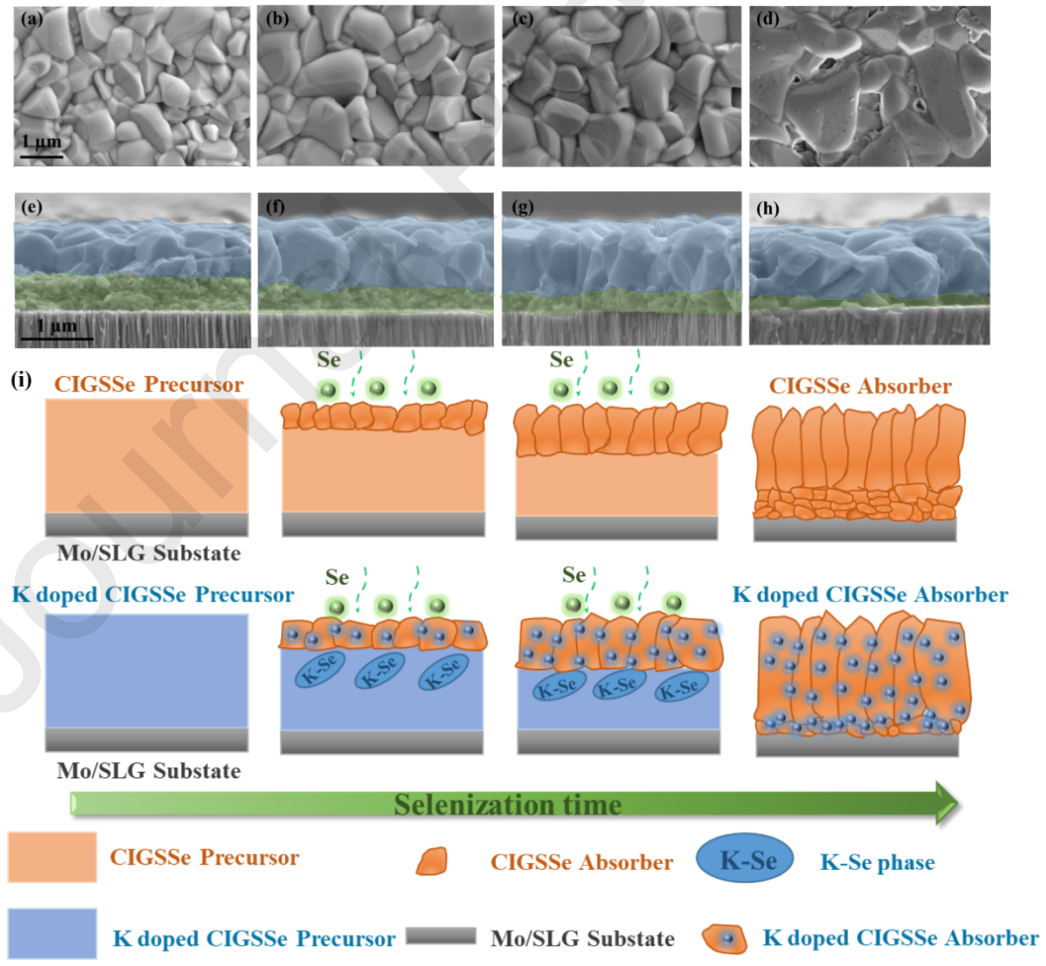


Fig. 3 The plane view (a-d) and cross-sectional (e-h) SEM images of K0, K1, K5 and

K10 CIGSSe absorbers; (i) Schematic illustration of the CIGSSe thin films growth mechanism for the un-doped and K-doped CIGSSe films during selenization process.

SEM was performed to investigate the morphology variation for different K doping contents. Fig. 3a-h displayed the surface and cross-section SEM images of CIGSSe films with different amounts K. As shown in Fig. 3a, the un-doped CIGSSe film exhibited large mount smaller size grains. After K doping, the grain size and uniformity of the K-doped CIGSSe films were found to be highly improved. However, excess amount of K induced some pinholes and voids on the surface of K10 CIGSSe absorber, which maybe was due to the segregation of K-related compounds in the absorber. All the CIGSSe films exhibited a typical double-layered structure consisting of upper large grains layer and bottom fine grains layer (Fig. 3e-h). This stratification is typically observed in solution-processed CIGSSe absorber layers.[5] The fine grain layer was originated from unwanted impurity elements from organic ligands and/or insufficient selenization, which will deteriorate device performance.[35] Fig. 3e showed that the fine grain layer of K0 CIGSSe film was about 450 nm. The thickness of fine grain layer in the CIGSSe thin films was gradually decreased with the increased K doping content (Fig. 3f-h). In K10 samples, the fine grain layer thickness was decreased to 140 nm. The above results confirmed that K doping indeed enlarges the crystal size and improves the CIGSSe crystallization. We speculated that the remarkable improvement in the absorber crystallization was ascribed to the formation of K-Se phase during chalcogenization as schematically illustrated in Fig. 3i. Because of the high chemical affinity of K and Se, the liquid Se-enriched K-Se phase was considered to be preferentially formed

Journal Pre-proofs

which will lower the melting point and promote grain growth.[24, 36] Meanwhile, the K-Se phase can serve as Se reservoir and form a Se-rich environment during the growth process, which result a more effective Se supply during selenization.[28] To reveal the existence of K-Se phase in the selenization process, we interrupt the selenization process and perform XPS measurement for the CIGSSe film which is selenized at 550 ℃ for 1 minute. As shown in Figure S3, the Se XPS peaks located at 53.4 eV and 54.3 eV were suggested to belong to the CIGSSe.[19] The peaks at higher binding energy of 54.9 and 55.5 eV were assigned to the K_2Se_3 phase.[37, 38] This result demonstrated the existence of K-Se phase in the selenization process. However, excess amount of K induced more pinholes and voids on the surface of K10 absorber, which maybe was due to the segregation of K-related compounds in the absorber. The Na element can helps crystal growth. However, the Na distribution was not obviously affected by the incorporation of K (Figure S4), indicating the improved crystallinity is mainly resulted from the K-doping effect. EDS was further performed to measure the elemental contents in K0 and K5 CIGSSe films. For each sample, we choosed three positions to check the elements composition (Figure S5).The results were presented in Table S1. Cu/(In+Ga) and Ga/(In+Ga) ratios were defined as CGI and GGI, respectively. For both K0 and K5 samples, the CGI and GGI ratios were all around 0.92 and 0.35, respectively. These were consistent with the ratios of elements in the precursor solution. From the EDS results, we can demonstrate that the elements composition was not affected by the K-doping.

XPS measurement was performed on K0 and K5 samples to examine the surface

state variation. As shown in Fig. 4a, the intensity of the Cu 2p peak for K5 CIGSSe sample was weaker than the K0 sample. This suggested that the surface Cu content was decreased after K doping. The decreased Cu content was proposed to increase the Cu vacancies (V_{Cu}) amount.[32, 36] Improved CIGSSe absorber crystallinity and increased V_{Cu} are positive factors for higher free carrier concentration, which is beneficial to the V_{OC}.[6, 39] The depletion of Cu was often observed in vacuum process prepared grown CIGSSe after KF-PDT.[40] The intensity of In 3d peaks and Ga 2p peaks were nearly unchanged after K doping (Fig. 4b, c). Fig. 4d, e showed the XPS data for the Se 3d core level for K0 CIGSSe film and K5 CIGSSe film. In both CIGSSe samples, the Se-1 XPS peaks (located at 53.4 eV and 54.3 eV) were observed. Se-1 signal has been suggested to belong to the CIGSSe chalcopyrite chemical environment.[19] For the K5 sample, we were able to identify an additional Se-2 bond at 53.1 and 53.9 eV, confirming the formation of new In-Se compounds (Fig. 4e).[41, 42] Fig. 4f, g showed the XPS spectra of the Se Auger-K 2p region. In K5 CIGSSe sample, an additional pair of XPS peaks at lower binding energy (located at 293.1 and 295.1 eV) was found, which was attributed to the K 2p photoelectron transition.[27] Combined with the changes in the Se-2 and K 2p XPS peaks, we considered the new In-Se compound as K-In-Se surface species. The K-In-Se phase was supposed to widen the bandgap at the CIGSSe surface and inhibit interface recombination at P-N junction.[39, 42] TOF-SIMS analysis was carried out to investigate the K distribution in the absorber film. Fig. 4h, i showed that the K0 and K5 devices exhibited similar depth profiles of Cu, In and Ga, suggesting the

incorporation of K does not obviously affect the distribution of these major elements. As mentioned in the experiment section, the KF was uniformly dissolved in the CIGSSe precursor solution. However, after selenization, the K element was not uniformly distributed in the CIGSSe film (Fig. 4i). It was reported that K tends to accumulate at the grain boundary and the CIGSSe surface.[24, 39] There were more grain boundaries in the bottom of the CIGSSe absorber, which was composed by small grains. Hence, K was enriched at the bottom of the absorber. Meanwhile, in the large grain region, the K content was gradually decreased toward the CIGSSe surface. It was noted that K also showed slightly enrichment on the surface, which could be attributed to the formation of K-In-Se phase. Additionally, the K-doping induced more uniform Cu distribution. The improved element distribution may decrease the bandgap fluctuation in CIGSSe films and it was proved by the following EQE results. Because the distribution of sulfur has a profound effect on the band gap grading, this is conducive to device performance. We further performed SIMS analysis of S and Se distribution. As shown in Figure S6, both the elemental S and Se are uniformly distributed throughout the absorber. This result further confirms that no sulfur grading is existed in the K5 CIGSSe absorber.

Journal Pre-proofs

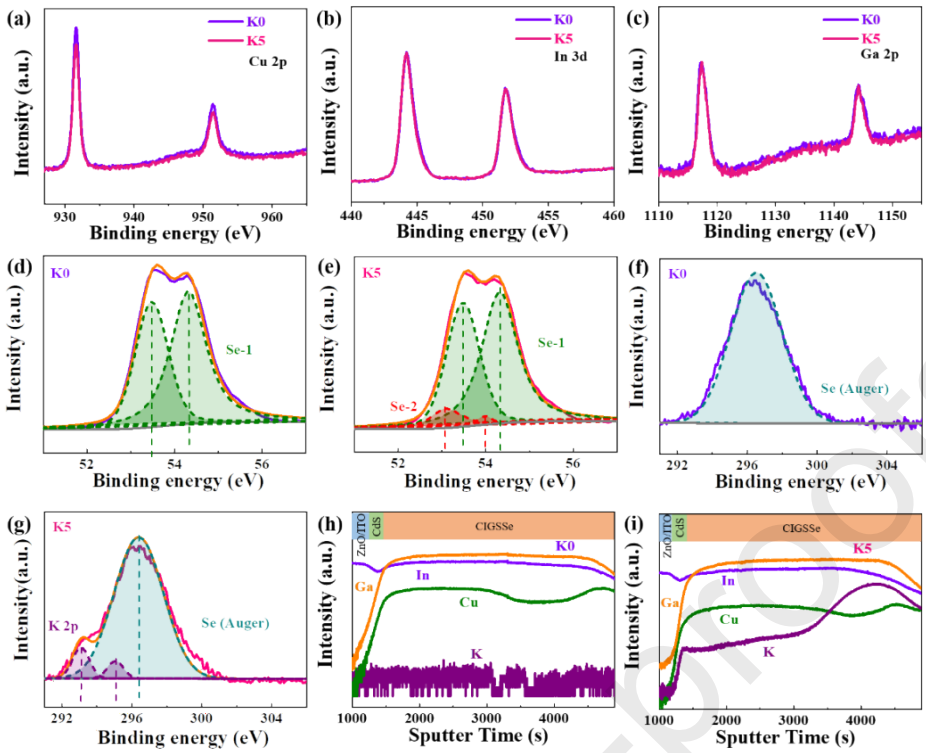


Fig. 4 The Cu 2p (a), In 3d (b), Ga 2p (c) XPS spectra of the K0 and K5 films; (d, e)Se Auger transitions and (f, g) K 2p photoelectron transitions of K0 and K5 film; TOF-SIMS elemental depth profiles of (h) K0 and (i) K5 device.

CIGSSe solar cells were fabricated to explore the effects of the amount of K added in the precursor solution on the device efficiencies. 20 devices for each condition were constructed to obtain the devices statistical. The statistical J_{SC}, V_{OC}, FF and PCE were presented in Fig. S7 (Supporting Information) and detailed values were summarized in Table 1. The best J-V curves of devices K0-K10 were shown in Fig.5a and the device parameters were listed in Table 1. In K-free CIGSSe absorber, the K0 device achieved average PCE of 12.79% with 620 mV of V_{OC}, 30.55 mA/cm^2 of J_{SC} and 67.66% of FF. The device efficiency was increased with an increase in the amount of K added. Excellent CIGSSe solar cell with optimized K amount of 5 mol‰ (K5) was obtained with a champion PCE of 16.02%, V_{OC} of 656 mV, J_{SC} of 33.61 mA/cm^2, and FF of 72.65%. To make a comparison, a survey of solution-processed

Journal Pre-proofs

CIGSSe solar cells based on alkali metal doping is summarized (Table 2). It is obvious that the in-suit K doped solution-process CIGSSe solar cell in this work exhibits the best PCE among them, confirming the benefits of K-doping. The Na-doping of CIGSSe absorber can passivate defects and promote the crystal growth of the absorber. In addition to passivating defects and promoting crystallinity, the K-doping can form K-In-Se phase to widen the CIGSSe surface bandgap and suppress the interface recombination. This is why K doping is more efficient than Na doping. In addition, the hybrid K/Na-doping was also a promising strategy to improve both bulk and surface properties. However, this doping process is complex and more efforts need to study. When excess amount of K (K10) was introduced, the average performance of K10 devices decreased to 13.69%. The reason for the deterioration of efficiency was caused by the pinholes on the surface of K10 samples (Fig. 3i), which may induce leakage and increase interface recombination.[46] The ideality factor (A), reverse saturation current density (J_0), serial (R_s) and shunt (R_{sh}) resistance were calculated from the J-V data. The K5 device exhibited the smallest A and J_0 values, demonstrating the lower recombination in both depletion region and absorber bulk.[47] Besides, the K5 device showed increased R_{sh} and decreased R_s compared with the K0 device (Table 1), indicating the improved FF.[6] Fig. 5b presented the EQE curves for the CIGSSe solar cells with different K amounts. The calculated J_{SC} from EQE (Fig. S8) were in good agreement with the J-V results. The results showed that the EQE response of K doped CIGSSe devices reflected better carrier collection efficiency than K-free device in long-wavelength ranges, confirming the higher J_{SC} in

K doped CIGSSe devices. This improvement suggests more efficient carrier collection capability, which may benefit from better crystallization and fewer defects in the K-doped CIGSSe bulk. The band gaps of the CIGSSe absorber films estimated from the EQE spectra (Fig. S9) were 1.243 eV for K5 device and 1.235 eV for K0 device, and this may be a reason for the increase in V_{OC}.[48] The band gap increment was 8 mV, but the V_{OC} for K5 device was 47 mV higher than K0 device, indicating the increased bandgap was not the decisive factor for V_{OC} improvement. Otherwise, the EQE response of K-doped CIGSSe devices showed sharp cut-off in the region between 900 and 1050 nm compared to the un-doped CIGSSe device. It indicated better band edge absorption of photons, which can be attributed to the decreased band tailing.[27] We further analyzed the derivative of the absorption spectrum extracted from the EQE spectra according to Mattheis′s methods.[49] The width parameter of a Gaussian fit to the derivative of the EQE spectrum represents the degree of bandgap fluctuations. As shown in Fig. 5c, the standard deviations (σ_{Eg}) of the bandgap fluctuation in K-doped CIGSSe devices were smaller than K-free CIGSSe devices. The K5 device displayed smallest σ_{Eg} of 21.5 eV, further demonstrating the highly decreased bandgap fluctuation in absorber. We inferred the likely reason for the reduction of bandgap fluctuations in K-doped CIGSSe was the suppressed formation of the In_{Cu} and Cu_{In} defects.[32, 33] We will discuss the K doping caused in the following section in detail. We further extracted the Urbach energy (E_U) to characterize the band tailing for different amount K doped CIGSSe absorbers (Fig. 5d).[9] The lowest E_U of 19.91 eV in K5 device confirmed a remarkable reduction in

Journal Pre-proofs

band-tailing and defects concentration. The smallest E_U also demonstrated the highest V_{OC} in the K5 device.

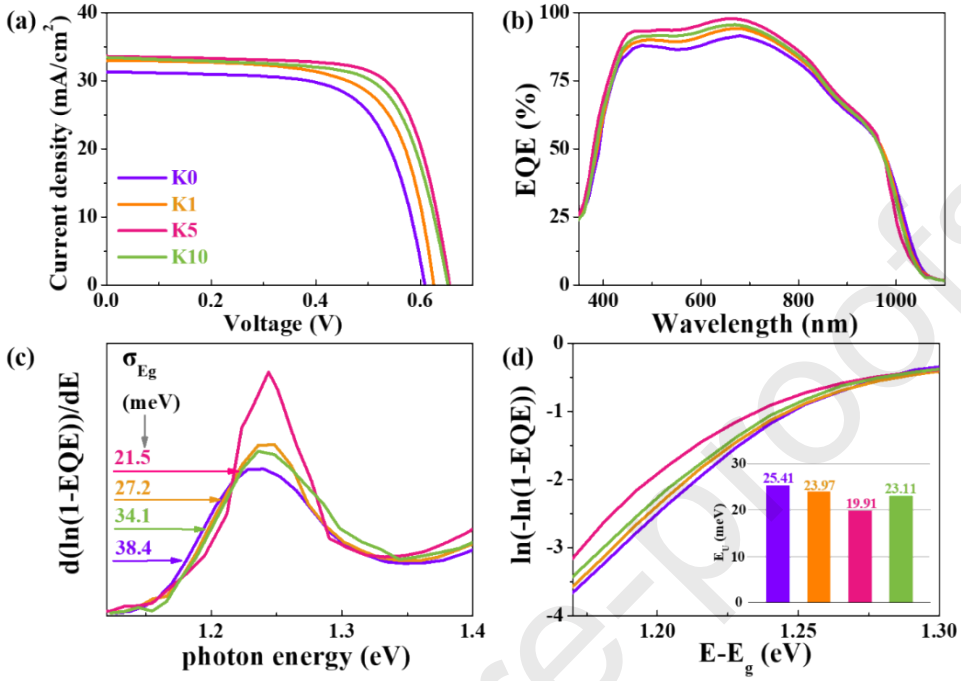


Fig. 5 (a) The current density-voltage and (b) the external quantum efficiency spectra of the K0-K10 devices; (c) extraction of the Urbach energy and (d) extraction of bandgap fluctuations of the absorbers from the EQE.

Table 1 Typical CIGSSe solar cells parameters of K0-K10 devices.

	J_{SC} (mA/cm²)	V_{OC} (mV)	FF (%)	PCE (%)	J_0 (mA/cm²)	A	R_s (Ω•cm²)	R_{sh} (Ω•cm²)
K0	31.31 (30.55±3.94)	609 (620±23)	68.01 (67.66±9.35)	12.96 (12.79±0.22)	7.35×10^{-5}	1.76	1.32	566.22
K1	32.52 (32.72±4.50)	630 (626±28)	70.02 (68.70±8.08)	14.34 (14.04±0.29)	1.58×10^{-5}	1.65	0.87	691.14
K5	33.61 (34.31±2.56)	656 (645±34)	72.65 (70.48±5.22)	16.02 (15.57±0.44)	5.70×10^{-6}	1.51	0.70	944.05
K10	33.45 (32.45±2.69)	629 (623±15)	66.96 (67.81±3.15)	14.08 (13.69±0.39)	8.91×10^{-6}	1.59	1.14	886.79

Table 2 The summary of solution-processed CIGSSe solar cells based on alkali metal doping.

Journal Pre-proofs

Reference	Solar cell type	Alkali source	Efficiency (%)	J_{SC} (mA/cm^2)	V_{OC} (V)	FF (%)
20	CIS	CH3COONa	12.83	38.59	0.49	67.74
26	CIGS	NaCl	10.3	26.8	0.6	63.6
27	CIGSSe	KF+NaF	12.0	30.8	0.62	63.3
28	CIGSSe	KF	15.0	33.1	0.62	73.5
29	CIGS	KF	11.02	31.8	0.54	64.61
43	CIS	CH3COONa	11.49	35.53	0.47	68.95
44	CIGSSe	NaCl	10.83	29.3	0.56	65.59
45	CIGS	NaF	6.7	30	0.48	46
This work	CIGSSe	KF	16.02	33.61	0.66	72.65

To evaluate the absorber and the interfaces properties in the K-doped and un-doped CIGSSe devices, C-V and DLCP measurements were utilized. The C-V and DLCP curves were shown in Fig. S10. The carrier densities versus distance to the junction interface extracted from C-V and DLCP curves were shown in Fig. 6a and Table 3. After K doping, the carrier density was slightly increased from 3.66×10^{16} (K0 device) to 6.84×10^{16} cm^{-3} (K5 device). The possible reason for the increased carrier density is the consuming or passivation of donor-like defects In-Cu antisite defects (In_{Cu}) by K doping in the bulk of the CIGSSe films.[32, 33] The larger carrier density contributed to the improved V_{OC} for K5 device. Because C-V response reflects free carriers, bulk and interface defects, whereas DLCP only represents responses from free carriers and bulk defects. Therefore, the interfacial defect density of the device can be calculated by subtracting N_{DL} (defect density calculated from DLCP measurement) from $N_{C\text{-}V}$ (defect density calculated from C-V

measurement).[47, 50, 51] The interface traps density for K5 CIGSSe device (2.60×10^{15} cm^{-3}) was lower than that of K0 device (6.01×10^{15} cm^{-3}). This dictated that the high density of interface defects in the un-doped device was significantly reduced after K doping. In addition, we performed DLCP measurements under different frequency. Since the defects cannot effectively respond to the excitation signals at high frequencies, the capacitance at high frequency only represents the response of the free carrier density, while the capacitance at low frequency represents the response of the sum of free carriers and deep traps.[52] DLCP data at high frequency yields an N_{DL} value only equal to the free-carrier density because the defects cannot effectively respond to the excitation signals at high frequencies. It means that DLCP data at low frequency yield an N_{DL} value equal to the sum of free-carrier density and the bulk defect density. DLCP data at high frequency yields an N_{DL} value only equal to the free-carrier density.[52, 53] Hence, disparity in high frequency and low frequency DLCP responses in principal was related to the bulk defect density. In K0 device, the difference was 5.53×10^{16} cm^{-3}, while the difference was 2.81×10^{16} cm^{-3} in K5 device. This revealed the bulk defects were also suppressed after K doping.

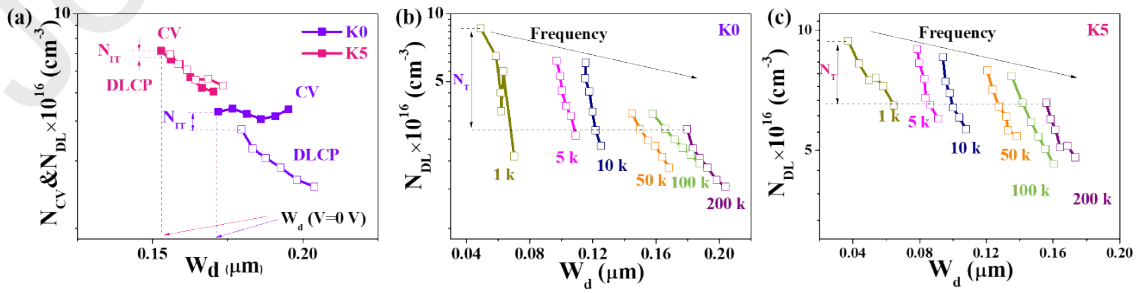


Fig. 6 (a) C-V and DLCP profiles for K0 and K5 device. DLCP measured at frequencies from 1 to 200 kHz for (b) K0 and (c) K5.

Table 3 Summary of the results derived from C-V and DLCP measurements. The activation energy and carrier lifetime are calculated from J-V-T and TPV measurement, respectively.

	N_{-CV} (cm^{-3})	N_{-DL} (cm^{-3})	Interface state response (relative values)	Bulk Defect density (cm^{-3})	Activation energy, E_A (eV)	τ_{TPV} (μs)
K0	3.66×10^{16}	3.06×10^{16}	6.01×10^{15}	5.53×10^{16}	0.768	2.22
K5	6.84×10^{16}	6.58×10^{16}	2.60×10^{15}	2.81×10^{16}	1.158	10.89

Capacitance-mode deep-level transient spectroscopy (C-DLTS) for the K0 and K5 devices was further utilized to get more information about defect properties in CIGSSe devices.[19, 54] Fig. 7a exhibited the DLTS spectra for both samples, and Fig. 7b showed the Arrhenius plot of each of the DLTS traps. The peaks with negative values in Fig. 7a were attributed to the hole emission (electron capture, defined as H1) from the majority-carrier hole trap, whereas the peaks with positive values were due to the electron emission (hole capture, defined as E1 and E2) from the minority-carrier electron trap.[54, 55] The trap activation energy (E_a) and defects density (N_T) for K0 and K5 device were derived by fitting the detected Arrhenius curves. As shown in Fig. 8a, three peaks located at 161 K (H1), 225 K (H2) and 282 K (E1) were clearly observed in K0 device, manifesting that three main defects were existed. The corresponding E_a for H1, H2 and E1 were 0.183, 0.277 (above the VBM) and 0.353 eV (below the CBM), respectively. In contrast, the K5 device exhibits H2 defects (at 224 K) and E1 defects (at 286 K). The E_a for H2 and E1 defects were 0.248 (above the VBM) and 0.341 eV (below the CBM), respectively. It was reported that the H1, H2 and E1 defects corresponded to deep V_{In}, Cu_{In} and In_{Cu} defects, respectively.[56] These defects are all deep defects, which are detrimental to the photovoltaic device efficiency. As shown in Fig. 7b and Table 4, the K5 devices

showed smaller E_a values, indicating a faster emission rate, and thus improving the carrier recombination induced energy loss.[57] V_{In} defects are commonly located in the intergranular region or grain boundary. As mentioned in the SEM results, the incorporation of K highly improved the absorber crystallization.[58] Thus V_{In} defects amount was suppressed due to decreased grain boundary numbers. This was why the V_{In} defects failed to defected in the K-doped device. During the CIGSSe film growing process, the K atom is more likely to occupy the Cu site than In (Ga) atom. The formation of donor point-defects is supposed to be inhibited by K substitution for the In_{Cu} or Cu_{In} antisites.[50] As a result, both the H2 (Cu_{In}) and E1 (In_{Cu}) defect density were remarkably decreased from 1.35×10^{14} and 6.77×10^{13} (K0 device) to 4.11×10^{13} and 2.94×10^{12} (K5 device), indicating the effective defects passivation effects of K doping. According to the above results, the reduced interface and bulk defects densities induced by incorporation of K in the CIGSSe absorber may significantly promote carrier collection efficiency and may also greatly contribute to the increase of efficiency by reducing the non-radiative recombination.

Journal Pre-proofs

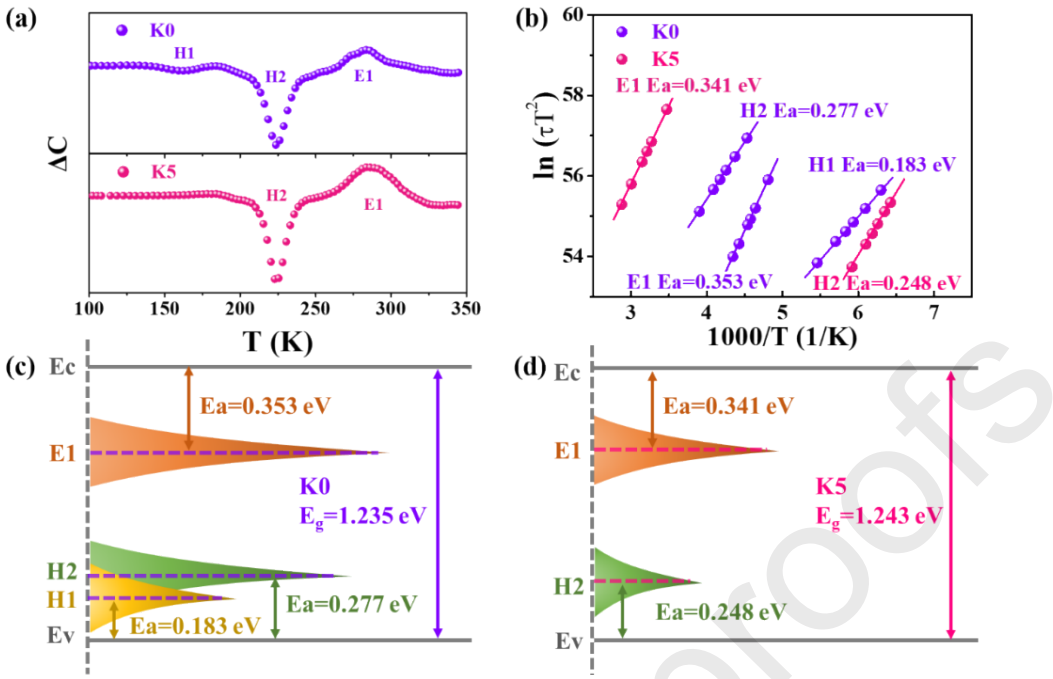


Fig. 7 (a) DLTS signals of K0 and K5 devices. ΔC is the variation of capacitance. (b) Arrhenius plots corresponding to the peaks derived from the DLTS spectra. (c), (d) Conduction band (Ec), valence band (Ev) and trap energy level (E_T) for K0 and K5 devices, the band gap was determined by the EQE (Fig. S9).

Table 4 Deep-level defect parameters (trap type, peak temperature, trap activate energy level (E_a), trap density (N_T), possible defect level) of K0 and K5 devices.

Device	Trap	Peak Temperature (K)	Activative energy E_a (eV)	Trap conc. N_T (cm^{-3})	Possible defect level
K0	H1	161	E_V+0.183	5.85×10^{12}	V_{In}
	H2	225	E_V+0.277	1.35×10^{14}	Cu_{In}
	E1	282	E_C-0.353	6.77×10^{13}	In_{Cu}
K5	H2	224	E_V+0.248	4.11×10^{13}	Cu_{In}
	E1	286	E_C-0.341	2.94×10^{12}	In_{Cu}

J-V-T curves were measured in the range of 90-350 K in the dark condition to elucidate underlying reasons for efficiency improvement for un-doped and K-doped CIGSSe devices. As shown in Fig. 8a, b, in K0 device, the exponential current increase in forward bias was largely restrained. This result demonstrated the strongly suppressed diode-like behavior in K0 device.[19] Whereas, the J-V-T curves of K5

Journal Pre-proofs

device exhibited good diode-like characteristics over the full temperature ranges.[10] Because the forward current contributes the main junction, the improved diode-like characteristics in lower temperature confirmed the better junction quality in K-doped device. Furthermore, we extracted the carrier recombination activation energy (E_A) from the dark J-V-T curves to determine the recombination path in K0 and K5 devices. According to the following equation:

$$\mathrm{Aln}(J_0) = \mathrm{Aln}(J_{00}) - \frac{E_A}{kT} \quad (1)$$

E_A can be determined by fitting the slope of versus 1/kT.[15, 59] The E_A value close to the absorber bandgap means that the bulk recombination is dominating. In contrast, the interface recombination is dominating when E_A value is smaller than absorber bandgap.[59] Fig. 8d showed that the E_A value of the K0 CIGSSe device was 0.768 eV, much smaller than the E_g of the K0 absorber (Fig. S9). This suggested that the recombination was occurred at the CIGSSe/CdS interface. The E_A value for the K5 device (1.158 eV) was close to the K5 absorber band gap (1.243 eV), which indicated bulk recombination predominates over interface recombination. The enhanced E_A value in K5 devices strongly demonstrated that the interface recombination was significantly passivated. We also extracted blocking barrier heights (Φ_B) from temperature-dependent Rs of these devices (Figure S11a) by using the thermal emission model.[60] As shown in Figure S10b, the K5 devices obtained lower Φ_B (115 meV for K5 device and 136 meV for the k0 device). It indicated the improved hole carriers transport to the Mo back contact after K-doping. However, these Φ_B values were high. More efforts need to decrease the carriers transport barrier for better

carrier transport. Transient photovoltage (TPV) measurement was utilized to further understand the interface carrier recombination in K0 and K5 devices. TPV spectra were obtained under open-circuit condition in the dark, as presented in Fig. 8d. According to the fitted results, the TPV lifetime (τ_{TPV}) increased from 2.22 to 10.89 μs for K0 and K5 solar cells, indicating the reduced carrier recombination of K5 device.[30] This result was consistent with the J-V-T result. The suppressed interface recombination in K5 device can be attributed the reduction of defects in absorber and modified CIGSSe surface. Furthermore, we employed electron beam induced current (EBIC) to achieve information about carrier collection mechanism (Figure S12). Figure R12e showed the normalized average EBIC signals along the brown dashed lines in Figure S12c,d. As shown in Figure S12e, for both samples, the EBIC signal was observed not only at the junction of CIGSSe/CdS interface but also at the CIGSSe/Mo interface. Obviously, the K5 device exhibits stronger EBIC signal. It demonstrated better carrier collection efficiency in the K-doped CIGSSe device.[6]

Journal Pre-proofs

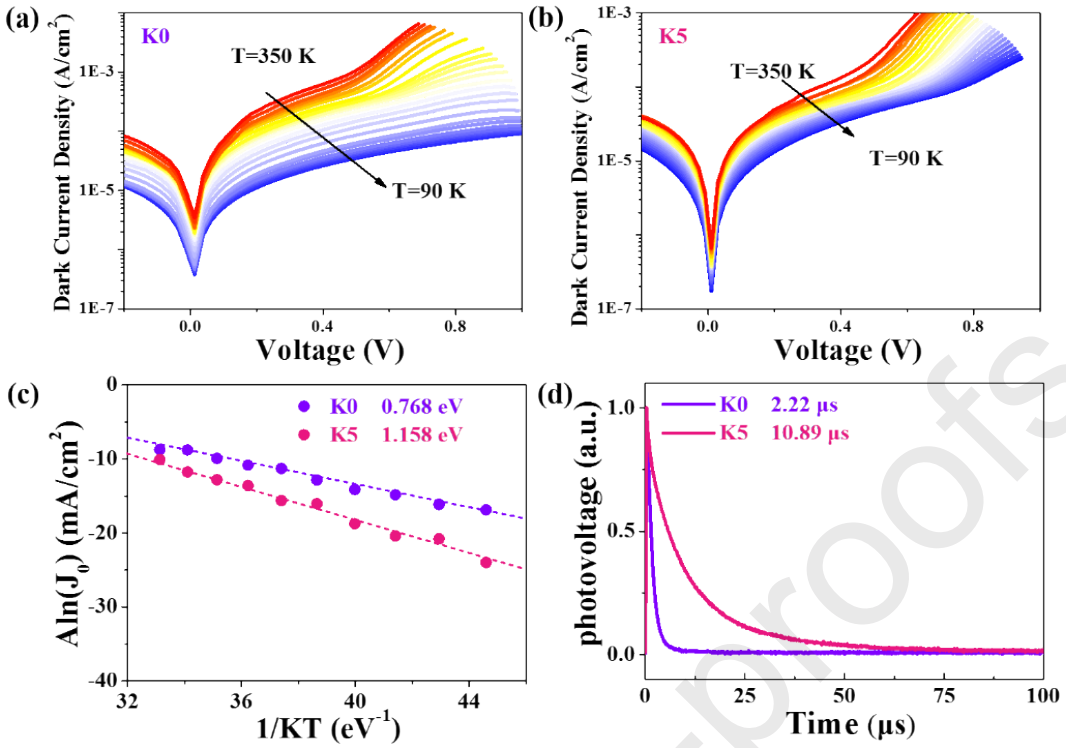


Fig. 8 Temperature-dependent dark current density vs voltage characteristics for a temperature range of approximately 320 to 90 K for (a) K0 device and (b) K5 device; (c) Aln(J_0) versus 1/kT plot of K0 and K5 device; (d) Transient photovoltage decay spectra of K0 and K5 device.

4. CONCLUSIONS

In summary, we demonstrated an effective and facile in-suit solution-based K doping strategy to prepare high-performance solution-processed CIGSSe solar cells. The effects of the K incorporation on the microstructure, electrical and physical properties of CIGSSe absorber were carefully investigated. Appropriate K incorporation induced highly improved the CIGSSe absorber crystallization, decreased Urbach energy and reduction of detrimental deep level defects. Meanwhile, the formation of K-In-Se phase on the CIGSSe surface could widen the surface bandgap and inhibit interface recombination. These positive effects have finally helped to promote the performance of the solution-processed CIGSSe solar cells reaching 16.02%, with improved V_{OC} of 655 mV and FF of 72.65%.

Journal Pre-proofs

Declaration of Interest Statement

The authors declare that they have no competing financial interests or personal relationships that could have appeared to influence the work reported in this paper.

Acknowledgements

Y. Zhao and Q. Gao contributed equally to this work. This work was supported by the National Natural Science Foundation of China (62104061, 62074052, U1904192, 61874159, 52072327, 51802081 and 61974173), the Key scientific and technological project of Henan Province (212300410115 and 20B480002), the Science and Technology Innovation Talents in Universities of Henan Province (21HASTIT023).

References

[1] N. Wu, Y. Li, M. Zeng, J. Gao, Y. Tang, Z. Zeng, Y. Zheng, Design of chalcopyrite-type $CuFeSe_2$ nanocrystals: Microstructure, magnetism, photoluminescence and sensing performances, J. Solid State Chem. 271 (2019) 292-297. https://doi.org/10.1016/j.jssc.2019.01.015.

[2] G. Liang, T. Liu, M. Ishaq, Z. Chen, R. Tang, Z. Zheng, Z. Su, P. Fan, X. Zhang, S. Chen, Heterojunction interface engineering enabling high onset potential in Sb_2Se_3/CdS photocathodes for efficient solar hydrogen production, Chem. Eng. J. (2021). https://doi.org/10.1016/j.cej.2021.133359.

[3] S.-C. Liu, C.-M. Dai, Y. Min, Y. Hou, A.H. Proppe, Y. Zhou, C. Chen, S. Chen, J. Tang, D.-J. Xue, E.H. Sargent, J.-S. Hu, An antibonding valence band maximum enables defect-tolerant and stable GeSe photovoltaics, Nat. Commun. 12(1) (2021). https://doi.org/10.1038/s41467-021-20955-5.

[4] X. Liu, J. Gao, Q. Wang, Structural-property correlations of all-inorganic $CsPbBr_3$ perovskites via synergetic controls by $PbBr_2$, 2-mercapto-3-methyl-4-thiazoleacetic acid and water, Chem. Eng. J. 428 (2022). https://doi.org/10.1016/j.cej.2021.131117.

Journal Pre-proofs

[5] S. Suresh, A.R. Uhl, Present Status of Solution-Processing Routes for Cu(In,Ga)$(S,Se)_2$ Solar Cell Absorbers, Adv. Energy Mater. 11(14) (2021) 2003743. https://doi.org/10.1002/aenm.202003743.

[6] Y. Zhao, S. Yuan, Q. Chang, Z. Zhou, D. Kou, W. Zhou, Y. Qi, S. Wu, Controllable Formation of Ordered Vacancy Compound for High Efficiency Solution Processed Cu(In,Ga)Se_2 Solar Cells, Adv. Funct. Mater. 31(10) (2020) 2007928. https://doi.org/10.1002/adfm.202007928.

[7] S. Siebentritt, E. Avancini, M. Bär, J. Bombsch, E. Bourgeois, S. Buecheler, R. Carron, C. Castro, S. Duguay, R. Félix, E. Handick, D. Hariskos, V. Havu, P. Jackson, H.P. Komsa, T. Kunze, M. Malitckaya, R. Menozzi, M. Nesladek, N. Nicoara, M. Puska, M. Raghuwanshi, P. Pareige, S. Sadewasser, G. Sozzi, A.N. Tiwari, S. Ueda, A. Vilalta-Clemente, T.P. Weiss, F. Werner, R.G. Wilks, W. Witte, M.H. Wolter, Heavy Alkali Treatment of Cu(In,Ga)Se_2 Solar Cells: Surface versus Bulk Effects, Adv. Energy Mater. 10(8) (2020) 1903752. https://doi.org/10.1002/aenm.201903752.

[8] M. Nakamura, K. Yamaguchi, Y. Kimoto, Y. Yasaki, T. Kato, H. Sugimoto, Cd-Free Cu(In,Ga)$(Se,S)_2$ Thin-Film Solar Cell With Record Efficiency of 23.35%, IEEE J. Photovolt. 9(6) (2019) 2156-3381. https://doi.org/10.1109/JPHOTOV.2019.2937218.

[9] R. Carron, S. Nishiwaki, T. Feurer, R. Hertwig, E. Avancini, J. Löckinger, S.C. Yang, S. Buecheler, A.N. Tiwari, Advanced Alkali Treatments for High-Efficiency Cu(In,Ga)Se_2 Solar Cells on Flexible Substrates, Adv. Energy Mater. 9(24) (2019) 1900408. https://doi.org/10.1002/aenm.201900408.

[10] F. Werner, M.H. Wolter, S. Siebentritt, G. Sozzi, S. Di Napoli, R. Menozzi, P. Jackson, W. Witte, R. Carron, E. Avancini, T.P. Weiss, S. Buecheler, Alkali treatments of Cu(In,Ga)Se_2 thin-film absorbers and their impact on transport barriers, Prog. Photovolt. 26(11) (2018) 911-923. https://doi.org/10.1002/pip.3032.

[11] T. Zhang, Y. Yang, D. Liu, S.C. Tse, W. Cao, Z. Feng, S. Chen, L. Qian, High efficiency solution-processed thin-film Cu(In,Ga)$(Se,S)_2$ solar cells, Energy Environ. Sci. 9(12) (2016) 3674-3681. https://doi.org/10.1039/c6ee02352e.

Journal Pre-proofs

[12] A.R. Uhl, A. Rajagopal, J.A. Clark, A. Murray, T. Feurer, S. Buecheler, A.K.Y. Jen, H.W. Hillhouse, Solution-Processed Low-Bandgap $CuIn(S,Se)_2$ Absorbers for High-Efficiency Single-Junction and Monolithic Chalcopyrite-Perovskite Tandem Solar Cells, Adv. Energy Mater. 8(27) (2018) 1801254. https://doi.org/10.1002/aenm.201801254.

[13] J. Ramanujam, U.P. Singh, Copper indium gallium selenide based solar cells–a review, Energy Environ. Sci. 10(6) (2017) 1306-1319. https://doi.org/10.1039/c7ee00826k.

[14] J. Jiang, R. Giridharagopal, E. Jedlicka, K. Sun, S. Yu, S. Wu, Y. Gong, W. Yan, D.S. Ginger, M.A. Green, X. Hao, W. Huang, H. Xin, Highly Efficient Copper-Rich Chalcopyrite Solar Cells from DMF Molecular Solution, Nano Energy 69 (2019) 104438. https://doi.org/10.1016/j.nanoen.2019.104438.

[15] G.S. Park, V.B. Chu, B.W. Kim, D.W. Kim, H.S. Oh, Y.J. Hwang, B.K. Min, Achieving 14.4% Alcohol-Based Solution-Processed $Cu(In,Ga)(S,Se)_2$ Thin Film Solar Cell through Interface Engineering, ACS Appl. Mater. Interfaces 10(12) (2018) 9894-9899. https://doi.org/10.1021/acsami.8b00526.

[16] T. Aramoto, Y. Kawaguchi, Y.-C. Liao, Y. Kikuchi, T. Ohashi, H. Iida, A. Nakamura, presented at 32nd European Photovoltaic Solar Energy Conf. and Exhibition, Munich, Germany, June 2016, pp. 1108–1111.

[17] N. Mufti, T. Amrillah, A. Taufiq, Sunaryono, Aripriharta, M. Diantoro, Zulhadjri, H. Nur, Review of CIGS-based solar cells manufacturing by structural engineering, Solar Energy 207 (2020) 1146-1157. https://doi.org/10.1016/j.solener.2020.07.065.

[18] M. Edoff, T. Jarmar, N.S. Nilsson, E. Wallin, D. Hogstrom, O. Stolt, O. Lundberg, W. Shafarman, L. Stolt, High Voc in $(Cu,Ag)(In,Ga)Se_2$ Solar Cells, IEEE J. Photovolt. 7 (2017) 1789-1794. https://doi.org/10.1109/JPHOTOV.2017.2756058.

[19] Y. Zhao, S. Yuan, D. Kou, Z. Zhou, X. Wang, H. Xiao, Y. Deng, C. Cui, Q. Chang, S. Wu, High Efficiency CIGS Solar Cells by Bulk Defect Passivation through Ag Substituting Strategy, ACS Appl. Mater. Interfaces 12(11) (2020) 12717-12726. https://doi.org/10.1021/acsami.9b21354.

Journal Pre-proofs

[20] S. Rehan, J. Moon, T.G. Kim, J. Gwak, J. Kim, J.W. Kim, W. Jo, S.K. Ahn, S. Ahn, Role of Na in solution-processed $CuInSe_2$ (CISe) devices: A different story for improving efficiency, Nano Energy 48 (2018) 401-412. https://doi.org/10.1016/j.nanoen.2018.03.065.

[21] Y. Sun, S. Lin, W. Li, S. Cheng, Y. Zhang, Y. Liu, W. Liu, Review on Alkali Element Doping in $Cu(In,Ga)Se_2$ Thin Films and Solar Cells, Engineering 3(4) (2017) 452-459. https://doi.org/10.1016/j.eng.2017.04.020.

[22] P. Jackson, R. Wuerz, D. Hariskos, E. Lotter, W. Witte, M. Powalla, Effects of heavy alkali elements in $Cu(In,Ga)Se_2$ solar cells with efficiencies up to 22.6%, Phys. Status Solidi Rapid Res. Lett. 10(8) (2016) 583-586. https://doi.org/10.1002/pssr.201600199.

[23] T. Kato, J.-L.Wu, Y. Hirai, H. Sugimoto, V. Bermudez, Record Efficiency for Thin-Film Polycrystalline Solar Cells Up to 22.9% Achieved by Cs-Treated $Cu(In,Ga)(Se,S)_2$, IEEE J. Photovolt. 9(1) (2019) 325-330. https://doi.org/10.1109/JPHOTOV.2018.2882206.

[24] M. Malitckaya, H.P. Komsa, V. Havu, M.J. Puska, Effect of Alkali Metal Atom Doping on the $CuInSe_2$-Based Solar Cell Absorber, J. Phys. Chem. C 121(29) (2017) 15516-15528. https://doi.org/10.1021/acs.jpcc.7b03083.

[25] Z.-K. Yuan, S. Chen, Y. Xie, J.-S. Park, H. Xiang, X.-G. Gong, S.-H. Wei, Na-Diffusion Enhanced p-type Conductivity in $Cu(In,Ga)Se_2$: A New Mechanism for Efficient Doping in Semiconductors, Adv. Energy Mater. 6(24) (2016) 1601191. https://doi.org/10.1002/aenm.201601191.

[26] S. Uličná, L.M. Welch, A. Abbas, M. Togay, V. Tsai, T.R. Betts, A.V. Malkov, J.M. Walls, J.W. Bowers, Sodium doping of solution-processed amine-thiol based CIGS solar cells by thermal evaporation of NaCl, Prog. Photovolt. 29(5) (2021) 546-557. https://doi.org/10.1002/pip.3408.

[27] E.H. Alruqobah, R. Agrawal, Potassium Treatments for Solution-Processed $Cu(In,Ga)(S,Se)_2$ Solar Cells, ACS Appl. Energy Mater. 3(5) (2020) 4821-4830. https://doi.org/10.1021/acsaem.0c00422.

[28] J.H. Kim, M.K. Kim, A. Gadisa, S.J. Stuard, M.M. Nahid, S. Kwon, S. Bae, B.

Journal Pre-proofs

Kim, G.S. Park, D.H. Won, D.K. Lee, D.W. Kim, T.J. Shin, Y.R. Do, J. Kim, W.J. Choi, H. Ade, B.K. Min, Morphological-Electrical Property Relation in $Cu(In,Ga)(S,Se)_2$ Solar Cells: Significance of Crystal Grain Growth and Band Grading by Potassium Treatment, Small 16(48) (2020) e2003865. https://doi.org/10.1002/smll.202003865.

[29] J.-C. Sung, C.-H. Lu, Potassium-ion doped $Cu(In,Ga)Se_2$ thin films solar cells: Phase formation, microstructures, and photovoltaic characteristics, Appl. Surf. Sci. 409 (2017) 270-276. https://doi.org/10.1016/j.apsusc.2017.03.020.

[30] S. Yuan, X. Wang, Y. Zhao, Q. Chang, Z. Xu, J. Kong, S. Wu, Solution Processed $Cu(In,Ga)(S,Se)_2$ Solar Cells with 15.25% Efficiency by Surface Sulfurization, ACS Appl. Energy Mater. 3(7) (2020) 6785-6792. https://doi.org/10.1021/acsaem.0c00917.

[31] D. Zhao, Q. Fan, Q. Tian, Z. Zhou, Y. Meng, D. Kou, W. Zhou, S. Wu, Eliminating fine-grained layers in $Cu(In,Ga)(S,Se)_2$ thin films for solution-processed high efficiency solar cells, J. Mater. Chem. A 4(35) (2016) 13476-13481. https://doi.org/10.1039/c6ta05728d.

[32] A. Laemmle, R. Wuerz, M. Powalla, Efficiency enhancement of $Cu(In,Ga)Se_2$ thin-film solar cells by a post-deposition treatment with potassium fluoride, Phys. Status Solidi Rapid Res. Lett. 7(9) (2013) 631-634. https://doi.org/10.1002/pssr.201307238.

[33] A. Laemmle, R. Wuerz, M. Powalla, Investigation of the effect of potassium on $Cu(In,Ga)Se_2$ layers and solar cells, Thin Solid Films 582 (2015) 27-30. https://doi.org/10.1016/j.tsf.2014.10.088.

[34] Z.Y. Xiao, B. Yao, Y.F. Li, Z.H. Ding, Z.M. Gao, H.F. Zhao, L.G. Zhang, Z.Z. Zhang, Y.R. Sui, G. Wang, Influencing Mechanism of the Selenization Temperature and Time on the Power Conversion Efficiency of $Cu_2ZnSn(S,Se)_4$-Based Solar Cells, ACS Appl. Mater. Interfaces 8(27) (2016) 17334-42. https://doi.org/10.1021/acsami.6b05201.

[35] S.G. Haass, M. Diethelm, M. Werner, B. Bissig, Y.E. Romanyuk, A.N. Tiwari, 11.2% Efficient Solution Processed Kesterite Solar Cell with a Low Voltage Deficit,

Journal Pre-proofs

Adv. Energy Mater. 5(18) (2015). https://doi.org/10.1002/aenm.201500712.

[36] I. Khatri, H. Fukai, H. Yamaguchi, M. Sugiyama, T. Nakada, Effect of potassium fluoride post-deposition treatment on Cu(In,Ga)Se_2 thin films and solar cells fabricated onto sodalime glass substrates, Sol. Energy Mater Sol. Cells 155 (2016) 280-287. https://doi.org/10.1016/j.solmat.2016.06.023.

[37] X. Zhou, P. Gao, S. Sun, D. Bao, Y. Wang, X. Li, T. Wu, Y. Chen, P. Yang, Amorphous, Crystalline and Crystalline/Amorphous Selenium Nanowires and Their Different (De)Lithiation Mechanisms, Chem. Mater. 27(19) (2015) 6730-6736. https://doi.org/10.1021/acs.chemmater.5b02753.

[38] M. Kim, G.D. Park, Y.C. Kang, Investigation of the potassium-ion storage mechanism of nickel selenide materials and rational design of nickel selenide-C yolk-shell structure for enhancing electrochemical properties, Int. J. Energy Res. (2021). https://doi.org/10.1002/er.7523.

[39] C.P. Muzzillo, Review of grain interior, grain boundary, and interface effects of K in CIGS solar cells: Mechanisms for performance enhancement, Sol. Energy Mater Sol. Cells 172 (2017) 18-24. https://doi.org/10.1016/j.solmat.2017.07.006.

[40] A. Chirila, P. Reinhard, F. Pianezzi, P. Bloesch, A.R. Uhl, C. Fella, L. Kranz, D. Keller, C. Gretener, H. Hagendorfer, D. Jaeger, R. Erni, S. Nishiwaki, S. Buecheler, A.N. Tiwari, Potassium-induced surface modification of Cu(In,Ga)Se_2 thin films for high-efficiency solar cells, Nat. Mater. 12(12) (2013) 1107-1111. https://doi.org/10.1038/nmat3789.

[41] T. Lepetit, S. Harel, L. Arzel, G. Ouvrard, N. Barreau, Coevaporated $KInSe_2$: A Fast Alternative to KF Postdeposition Treatment in High-Efficiency Cu(In,Ga)Se_2 Thin Film Solar Cells, IEEE J. Photovolt. 6(5) (2016) 1316-1320. https://doi.org/10.1109/jphotov.2016.2589365.

[42] E. Handick, P. Reinhard, J.H. Alsmeier, L. Kohler, F. Pianezzi, S. Krause, M. Gorgoi, E. Ikenaga, N. Koch, R.G. Wilks, S. Buecheler, A.N. Tiwari, M. Bar, Potassium Postdeposition Treatment-Induced Band Gap Widening at Cu(In,Ga)Se_2 Surfaces-Reason for Performance Leap?, ACS Appl. Mater. Interfaces 7(49) (2015) 27414-27420. https://doi.org/10.1021/acsami.5b09231.

Journal Pre-proofs

[43] J. Moon, S. Rehan, T.R. Rana, B. O, S.K. Ahn, S. Ahn, Na-Induced Conversion of a Notorious Fine-Grained Residue Layer into a Working Absorber in Solution-Processed $CuInSe_2$ Devices, Solar RRL 3(11) (2019) 1900260. https://doi.org/10.1002/solr.201900260.

[44] M. Wang, M.A. Hossain, K.L. Choy, Effect of Sodium Treatment on the Performance of Electrostatic Spray Assisted Vapour Deposited Copper-poor $Cu(In,Ga)(S,Se)_2$ Solar Cells, Sci. Rep. 7(1) (2017) 6788. https://doi.org/10.1038/s41598-017-07027-9.

[45] A.C. Badgujar, R.O. Dusane, S.R. Dhage, $Cu(In,Ga)Se_2$ thin film solar cells produced by atmospheric selenization of spray casted nanocrystalline layers, Solar Energy 209 (2020) 1-10. https://doi.org/10.1016/j.solener.2020.08.080.

[46] X. Zheng, H. Lei, G. Yang, W. Ke, Z. Chen, C. Chen, J. Ma, Q. Guo, F. Yao, Q. Zhang, H. Xu, G. Fang, Enhancing efficiency and stability of perovskite solar cells via a high mobility p-type PbS buffer layer, Nano Energy 38 (2017) 1-11. https://doi.org/10.1016/j.nanoen.2017.05.040.

[47] Y. Gong, Y. Zhang, Q. Zhu, Y. Zhou, R. Qiu, C. Niu, W. Yan, W. Huang, H. Xin, Identify the origin of the Voc deficit of kesterite solar cells from the two grain growth mechanisms induced by Sn^{2+} and Sn^{4+} precursors in DMSO solution, Energy Environ. Sci. 14(4) (2021) 2369-2380. https://doi.org/10.1039/d0ee03702h.

[48] M. He, X. Zhang, J. Huang, J. Li, C. Yan, J. Kim, Y.S. Chen, L. Yang, J.M. Cairney, Y. Zhang, S. Chen, J. Kim, M.A. Green, X. Hao, High Efficiency $Cu_2ZnSn(S,Se)_4$ Solar Cells with Shallow Li_{Zn} Acceptor Defects Enabled by Solution-Based Li post-Deposition Treatment, Adv. Energy Mater. 11(13) (2021) 2003783. https://doi.org/10.1002/aenm.202003783.

[49] J. Mattheis, U. Rau, J.H. Werner, Light absorption and emission in semiconductors with band gap fluctuations-A study on $Cu(In,Ga)Se_2$ thin films, J. Appl. Phys. 101(11) (2007) 113519. https://doi.org/10.1063/1.2721768.

[50] M.A. Contreras, B. Egaas, P. Dippo, J. Webb, J. Granata, K. Ramanathan, S. Asher, A. Swartzlander, R. Noufi, On the Role of Na and Modifications to $Cu(In,Ga)Se_2$ Absorber Materials Using Thin-MF (M=Na, K, Cs) Precursor Layers,

Journal Pre-proofs

Presented at the 26th IEEE Photovoltaic Specialists Conference (1997). https://doi.org/10.1109/PVSC.1997.654102.

[51] Z. Su, G. Liang, P. Fan, J. Luo, Z. Zheng, Z. Xie, W. Wang, S. Chen, J. Hu, Y. Wei, C. Yan, J. Huang, X. Hao, F. Liu, Device Postannealing Enabling over 12% Efficient Solution-Processed Cu_2ZnSnS_4 Solar Cells with Cd^{2+} Substitution, Adv. Mater. 32(32) (2020) e2000121. https://doi.org/10.1002/adma.202000121.

[52] P. K. Johnson, J.T. Heath, J.D. Cohen, K. Ramanathan, J.R. Sites, A comparative study of defect states in evaporated and selenized CIGS(S) solar cells, Prog. Photovolt. 13(7) (2005) 579-586. https://doi.org/10.1002/pip.619.

[53] L. Yin, G. Cheng, Y. Feng, Z. Li, C. Yang, X. Xiao, Limitation factors for the performance of kesterite Cu_2ZnSnS_4 thin film solar cells studied by defects characterization, RSC Adv. 5(50) (2015) 40369-40374. https://doi.org/10.1039/C5RA00069F.

[54] I.-H. Choi, C.-H. Choi, J.-W. Lee, Deep centers in a $CuInGaSe_2$/CdS/ZnO:B solar cell, Phys. Status Solidi A 209(6) (2012) 1192-1197. https://doi.org/10.1002/pssa.201127596.

[55] R. Tang, X. Wang, W. Lian, J.g Huang, Q. Wei, M. Huang, Y. Yin, C. Jiang, S. Yang, G. Xing, S. Chen, C. Zhu, X. Hao, M. A. Green, T. Chen, Hydrothermal deposition of antimony selenosulfide thin films enables solar cells with 10% efficiency, Nat. Energy 5 (2020) 587-595. https://doi.org/10.1038/s41560-020-0652-3.

[56] S.-H. Wei, S.B. Zhang, A. Zunger, Effects of Ga addition to $CuInSe_2$ on its electronic, structural, and defect properties, Appl. Phys. Lett. 72(24) (1998) 3199-3201. https://doi.org/10.1063/1.121548.

[57] H.-S. Duan, W. Yang, B. Bob, C.-J. Hsu, B. Lei, Y. Yang, The Role of Sulfur in Solution-Processed $Cu_2ZnSn(S,Se)_4$ and its Effect on Defect Properties, Adv. Funct. Mater. 23(11) (2013) 1466-1471. https://doi.org/10.1002/adfm.201201732.

[58] P.K. Paul, K. Aryal, S. Marsillac, S.A. Ringel, A.R. Arehart, Impact of the Ga/In ratio on defects in $Cu(In,Ga)Se_2$, 2016 IEEE 43rd Photovoltaic Specialists Conference (PVSC) (2016) 2246-2249. https://doi.org/10.1063/1.3567006.

Journal Pre-proofs

[59] K.-J. Yang, J.-H. Sim, B. Jeon, D.-H. Son, D.-H. Kim, S.-J. Sung, D.-K. Hwang, S. Song, D.B. Khadka, J. Kim, J.-K. Kang, Effects of Na and MoS_2 on Cu_2ZnSnS_4 thin-film solar cell, Prog. Photovolt. 23(7) (2015) 862-873. https://doi.org/10.1002/pip.2500.

[60] O. Gunawan, T. K. Todorov, D. B. Mitzi, Loss mechanisms in hydrazine-processed Cu2ZnSn(Se,S)$_4$ solar cells, Appl. Phys. Lett. 97 (2010), 233506. http://dx.doi.org/10.1063/1.3522884.

Highlights

- Introducing KF into the CIGSSe precursor solution to improve the crystallization and passivate the deep defects.
- The effects of K on the solution-processed CIGSSe devices are systematic investigated.
- The band-tailing effect is reduced, deep-level defects are suppressed, and interface recombination is passivated.
- The solution-processed CIGSSe solar cell achieves high efficiency of 16.02%.

Journal Pre-proofs